

PAPER • OPEN ACCESS

## $\text{Ni}_3\text{S}_4/\text{NiS}/\text{rGO}$ as a promising electrocatalyst for methanol and ethanol electro-oxidation

To cite this article: Sadegh Azizi *et al* 2023 *Nano Futures* 7 015002

View the [article online](#) for updates and enhancements.

You may also like

- [Mapping critical natural capital at a regional scale: spatiotemporal variations and the effectiveness of priority conservation](#)

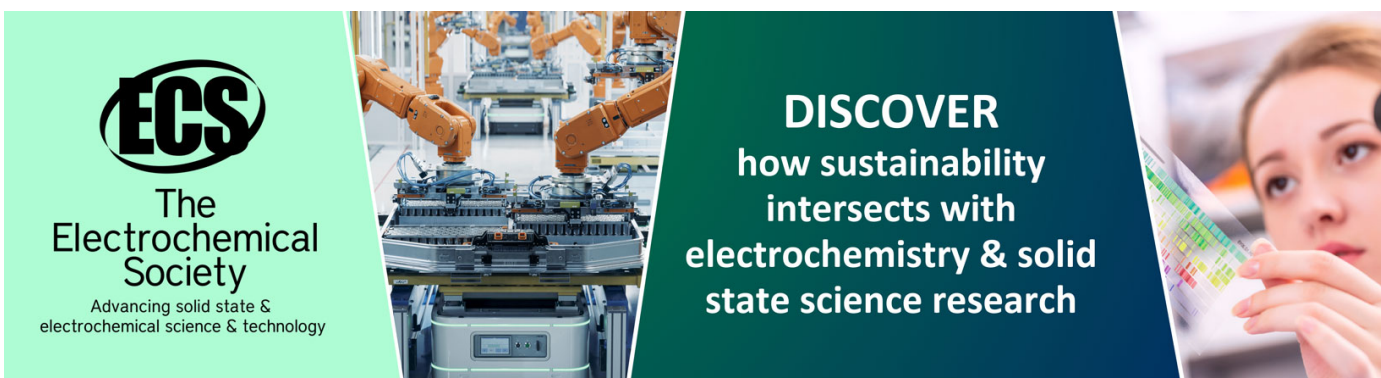
Yuanxin Liu, Yihe Lü, Wei Jiang *et al.*

- [Twin neural network regression is a semi-supervised regression algorithm](#)

Sebastian J Wetzel, Roger G Melko and Isaac Tamblyn

- [The NuSTAR Hard X-Ray Survey of the Norma Arm Region](#)

Francesca M. Fornasini, John A. Tomsick, JaeSub Hong *et al.*



**ECS**  
The  
Electrochemical  
Society  
Advancing solid state &  
electrochemical science & technology

**DISCOVER**  
how sustainability  
intersects with  
electrochemistry & solid  
state science research

## OPEN ACCESS

RECEIVED  
19 September 2022REVISED  
1 December 2022ACCEPTED FOR PUBLICATION  
3 January 2023PUBLISHED  
31 January 2023

Original content from this work may be used under the terms of the [Creative Commons Attribution 4.0 licence](#).

Any further distribution of this work must maintain attribution to the author(s) and the title of the work, journal citation and DOI.



## PAPER

# Ni<sub>3</sub>S<sub>4</sub>/NiS/rGO as a promising electrocatalyst for methanol and ethanol electro-oxidation

Sadegh Azizi<sup>1</sup>, Mohammad Bagher Askari<sup>2,\*</sup>, Mohammad Taghi Tourchi Moghadam<sup>1</sup>, Majid Seifi<sup>1</sup> and Antonio Di Bartolomeo<sup>3,\*</sup><sup>1</sup> Department of Physics, Faculty of Science, University of Guilan, PO Box 41335-1914, Rasht, Iran<sup>2</sup> Department of Semiconductor, Institute of Science and High Technology and Environmental Sciences, Graduate University of Advanced Technology, PO Box 7631818356, Kerman, Iran<sup>3</sup> Department of Physics 'E. R. Caianiello' and 'Interdepartmental Center NANOMATES', University of Salerno, Fisciano, Salerno 84084, Italy

\* Authors to whom any correspondence should be addressed.

E-mail: [mbaskari@phdguilan.ac.ir](mailto:mbaskari@phdguilan.ac.ir) and [adibartolomeo@unisa.it](mailto:adibartolomeo@unisa.it)**Keywords:** graphene, nanostructure, catalytic, electrochemical synthesis, ethanol, oxidation

## Abstract

We present a one-step hydrothermal synthesis of hybrids consisting of nickel sulfides in the form of Ni<sub>3</sub>S<sub>4</sub>-NiS (NN) and Ni<sub>3</sub>S<sub>4</sub>-NiS-rGO (NNR), i.e. with the addition of reduced graphene oxide (rGO), for application as catalysts. After accurate physical characterization and confirmation of successful synthesis, we evaluate the ability of these catalysts in the processes of methanol and ethanol oxidation. The precise electrochemical analyses show relatively good potential and excellent cyclic stability in methanol oxidation reaction (MOR) and ethanol oxidation reaction (EOR) processes. The comparison of the two catalysts shows the superiority of NNR over NN, confirming that rGO introduces a higher specific surface area and a higher electrical conductivity in the NNR structure. In the process of MOR, NNR has an oxidation peak at a current density of 55 mA cm<sup>-2</sup> and a peak potential of 0.54 V. In EOR, this peak is located at a current density of 11 mA cm<sup>-2</sup> and at a peak potential of 0.59 V. NNR has 97% and 94% stability in MOR and EOR after 1000 consecutive cycles, respectively, which are acceptable values.

## 1. Introduction

The huge fossil fuel consumption and the consequent increase of CO<sub>2</sub> in the atmosphere [1] is concentrating the attention of researchers toward renewable energy sources for the conversion and production of energy [2]. Among the modern and advanced devices for energy production and storage, we can mention all types of fuel cells, supercapacitors, and types of electrochemical batteries. Among the most important components of these devices are the catalysts and electrode materials used in their structure. A fuel cell converts chemical energy into electrical energy [3], and consists of three parts; the anode, the cathode, and the polymer membrane that is placed between the anode and cathode and is responsible for proton exchange [4]. One of the concerns of catalyst science, especially in the field of designing and manufacturing high-efficiency catalysts for use in the anode and cathode of fuel cells, is the synthesis of affordable and sustainable materials for the industrialization of these modern and attractive devices. In addition to having high electrocatalytic activity, catalysts should also have a suitable electrochemical active surface area and acceptable electrical conductivity [5].

Direct alcohol fuel cells with high efficiency, low operating temperature, environmental friendliness, and green energy sources are promising candidates to replace fossil fuel sources [6]. Despite several positive features, the slow kinetics of the methanol oxidation reaction (MOR), ethanol oxidation reaction (EOR), oxygen evolution reaction (OER), and catalyst poisoning are barriers to the commercialization and industrialization of alcohol fuel cells [7–10]. So far, platinum and its compounds are the best catalysts for use in methanol and ethanol oxidation for application in the anode of alcohol fuel cells [11]. However, the high price and toxicity at moderate temperature do not allow Pt and its compounds to be used as easy and

cost-effective materials [12, 13]. These drawbacks have led researchers to find alternative materials. Recently, it has been shown that transition metal oxides [14–16] and transition metal sulfides [17, 18] are promising for use in the anodic structure of catalysts due to their low cost and high cyclic stability performance in MOR and EOR [19, 20]. Specifically, nickel sulfide is a cost-effective catalyst [21] that has shown excellent performance in the processes of hydrogen evolution reaction [22], OER [23], supercapacitors [24], water oxidation [25], electrochemical sensors [26], and electrochemical batteries [27–29]. Despite these encouraging results, there are still few research efforts that have investigated nickel sulfide-based material in the MOR process.

The use of different types of carbon in the structure of catalysts, considering the abundance of this element in nature and also improving the electrocatalytic performance of catalysts, can be an attractive option for the synthesis of inexpensive, stable catalysts with excellent mechanical and electrochemical properties. Among the types of these carbon structures, we can mention reduced graphene oxide (rGO), multi-walled carbon nanotubes (MWCNTs), single-walled carbon nanotubes, carbon structures obtained from biomass, activated carbon, hollow carbon nanospheres, and recently graphdiyne [30, 31].

As the morphology, structure, conductivity, and specific surface area are the important and effective factors in the catalytic performance [32], in this study, we succeeded in synthesizing  $\text{Ni}_3\text{S}_4\text{-NiS}$  (NN) catalysts with starfish morphology using an easy and low-cost hydrothermal method. In the next step, we used rGO to produce  $\text{Ni}_3\text{S}_4\text{-NiS-rGO}$  (NNR) hybrids that provide a higher surface area. The rGO nanosheets, as a high-strength structure with a large surface area and high electrical conductivity, increase the catalyst stability in the alcohol process [33]. In this work, we show that both NN and NNR possess adequate catalytic performance for alcohol oxidation to be promising for use in the anode of alcohol fuel cells. It is noteworthy that in a previous study we investigated the potential of these catalysts as supercapacitor electrodes, demonstrating their great potential in electrochemical energy storage devices [34].

## 2. Experiment

### 2.1. Materials and instruments

All chemical precursors, such as deionized water, pristine graphite, potassium permanganate, hydrochloric acid, sulfuric acid, hydrogen peroxide, phosphoric acid, nickel nitrate hexahydrate ( $\text{Ni}(\text{NO}_3)_2 \cdot 6\text{H}_2\text{O}$ ), polyvinylidene fluoride, N-methyl pyrrolidone, and thiourea ( $\text{CH}_4\text{N}_2\text{S}$ ), were purchased with high purification from MERK Company. The crystalline structure of the prepared samples was analyzed using an x-ray diffraction (XRD, PHILIPS PW1730) model with monochromatized  $\text{Cu-K}\alpha$  radiation ( $\lambda = 1.541874 \text{ \AA}$ ) at room temperature within the range of two thetas of  $20^\circ\text{--}70^\circ$ . Raman spectra were analyzed with a micro Raman spectrometer at 532 nm wavelengths (Takram N1-541). The morphology and structure of the synthesized samples were characterized by field emission scanning electron microscope (Mira3 XMU from TESCAN Company), transmission electron microscope (TEM, JEOL 2010), and an energy-dispersive x-ray analyzer.

### 2.2. Synthesis and characterization of NN and NNR

The synthesis of NN was performed using the hydrothermal method. To prepare NN, 5.4 mmol of  $\text{Ni}(\text{NO}_3)_2 \cdot 6\text{H}_2\text{O}$  was dissolved in a 35 ml mix of ethanol and distilled water. Afterwards, 2.4 mmol of  $\text{CH}_4\text{N}_2\text{S}$  was added dropwise into the solution until the final color turned green and then stirred for 30 min. Simultaneously, a  $1 \times 1 \text{ cm}^2$  piece of cleaned nickel foam (NF) was immersed in the prepared solution. Finally, suspensions were sealed into a Teflon-lined autoclave and maintained at  $180^\circ\text{C}$  for 21 h. Subsequently, the autoclave was cooled to room temperature naturally. The resulting samples were washed several times with distilled water and finally with ethanol to remove the impurities and dried at  $50^\circ\text{C}$  in a vacuum oven. In this research, four samples were synthesized, including NN (S1) (sample without rGO) and three samples of NNR with 0.03 (S2), 0.05 (S3), and 0.07 (S4) grams of GO added to the precursors.

The synthesis method of NNR with the optimal amount of GO was almost the same as that of NN, with the difference that we added 0.05 grams of GO to the precursors at the beginning of the synthesis [34]. It should be mentioned that the optimal sample had the best electrochemical results in the process of methanol and ethanol oxidation.

### 2.3. Electrochemical test on NN and NNR catalysts

A three-electrode system was used for electrochemical analysis. A platinum wire with a diameter of 0.5 mm was used as an auxiliary electrode and the Ag/AgCl electrode was our reference electrode. The modified NN and NNR on NF ( $1 \times 1 \text{ cm}$ ) was our working electrode to investigate the capability of NN and NNR in the methanol and ethanol oxidation process that takes place in the anode of the fuel cell.

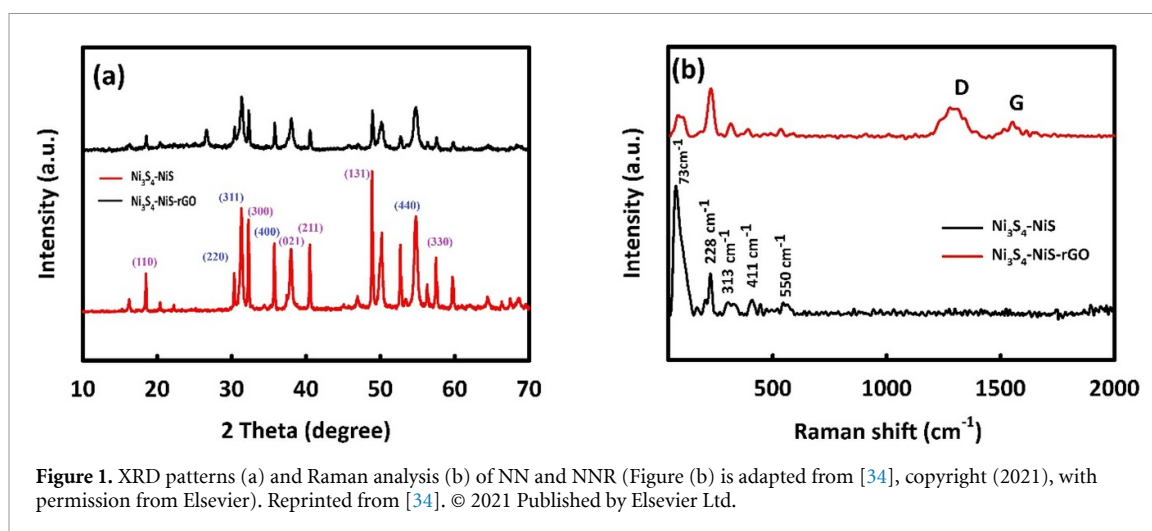


**Figure 1.** XRD patterns (a) and Raman analysis (b) of NN and NNR (Figure (b) is adapted from [34], copyright (2021), with permission from Elsevier). Reprinted from [34]. © 2021 Published by Elsevier Ltd.

### 3. Results and discussion

The XRD patterns of NN and NN with an optimized amount of rGO (NNR) are shown in figure 1(a). According to the patterns, the significant peaks of NiS can be observed at  $2\theta$  equal to 18.44, 32.2, 35.7, 40.45, 48.84, and 57.41°, which matches with the (110), (300), (021), (211), (131), and (330) crystal planes. All the XRD peaks for the sample were indexed by the rhombohedral structure with the reported data (JCPDS No. 000120041). Also, for Ni<sub>3</sub>S<sub>4</sub>, we have significant peaks at  $2\theta$  equal to 26.6, 31.34, 38.03, and 54.87°, related to (220), (311), (400), and (440) indexed by the cubic phase with *fd3m* structure, consistent with the reported data (JCPDS No. 010761813). Using the Debye–Scherrer equation ( $D = 0.9\lambda/\beta\cos\theta$ ), the average crystal size of NN was 68.6 nm. In addition, in the NNR XRD pattern, we almost see the characteristic peaks of NN. The addition of rGO reduced the intensity of the peaks, and a weak peak at around 26 degrees appeared that is attributed to the presence of rGO [34].

Raman analysis can reveal the structure of carbon-based materials and was employed to indicate the presence and quality of carbon in the structure of the catalyst. Figure 1(b) shows the Raman spectra of NN and NNR. The NNR spectra show significant peaks of graphene at 1300 and 1570  $\text{cm}^{-1}$ , which are related to the D and G bands of graphene. The D band refers to an asymmetric state called A<sub>1g</sub> that corresponds to phonons near the K region, and the G band is related to the sp<sup>2</sup> structure of the graphite plate, which appears as E<sub>2g</sub> in active Raman modes. Peaks also appeared at around 411, 313, 228, and 73  $\text{cm}^{-1}$  in both samples due to NN [34].

The surface morphologies of all the synthesized samples (S1–S4), as well as an SEM image of the rGO nanosheets, are shown in figures 2(a)–(o), respectively. Three SEM images of each sample are shown in the figure. The SEM images of 2(a)–(c) are related to the NN sample, which has a uniform starfish-like morphology.

The SEM images of S2 are shown in figures 2d–f. Figures 2g–i and figures 2j–l are the SEM images of S3 and S4, respectively.

SEM images of graphene nanosheets are also shown in figures 2(m)–(o). The sheet and two-dimensional morphology of these materials are also clearly visible in the images.

EDS mapping analysis was performed to examine the presence of elements. Figure 3 clearly shows the presence of nickel, sulfur, and carbon in the synthesized nano-hybrids, and also confirms the almost uniform distribution of NN nanoparticles on the graphene surface [34].

TEM images of rGO, NN (at two scales), and NNR are shown in figure 4. Figure 4(a) shows the very transparent plate morphology of the rGO nanosheets at the scale of 100 nm. In figures 4(b) and (c), the NN with its special morphology is visible at the scale of 2  $\mu\text{m}$ . Due to the large size of NN, its unique morphology is difficult to observe in the TEM image at a very low scale. Figure 4(d) shows a corner of the NN placed on the transparent rGO surface.

#### 3.1. Electrochemical investigation on NN and NNR catalysts for MOR process

For this purpose, first, 1 M KOH solution was prepared, and cyclic voltammetry (CV) analysis of the modified electrodes was performed. As figure 5(a) shows, the addition of rGO to the NN structure increased the current density of the hybrid catalyst. rGO as a conductive material with a high active surface area has a

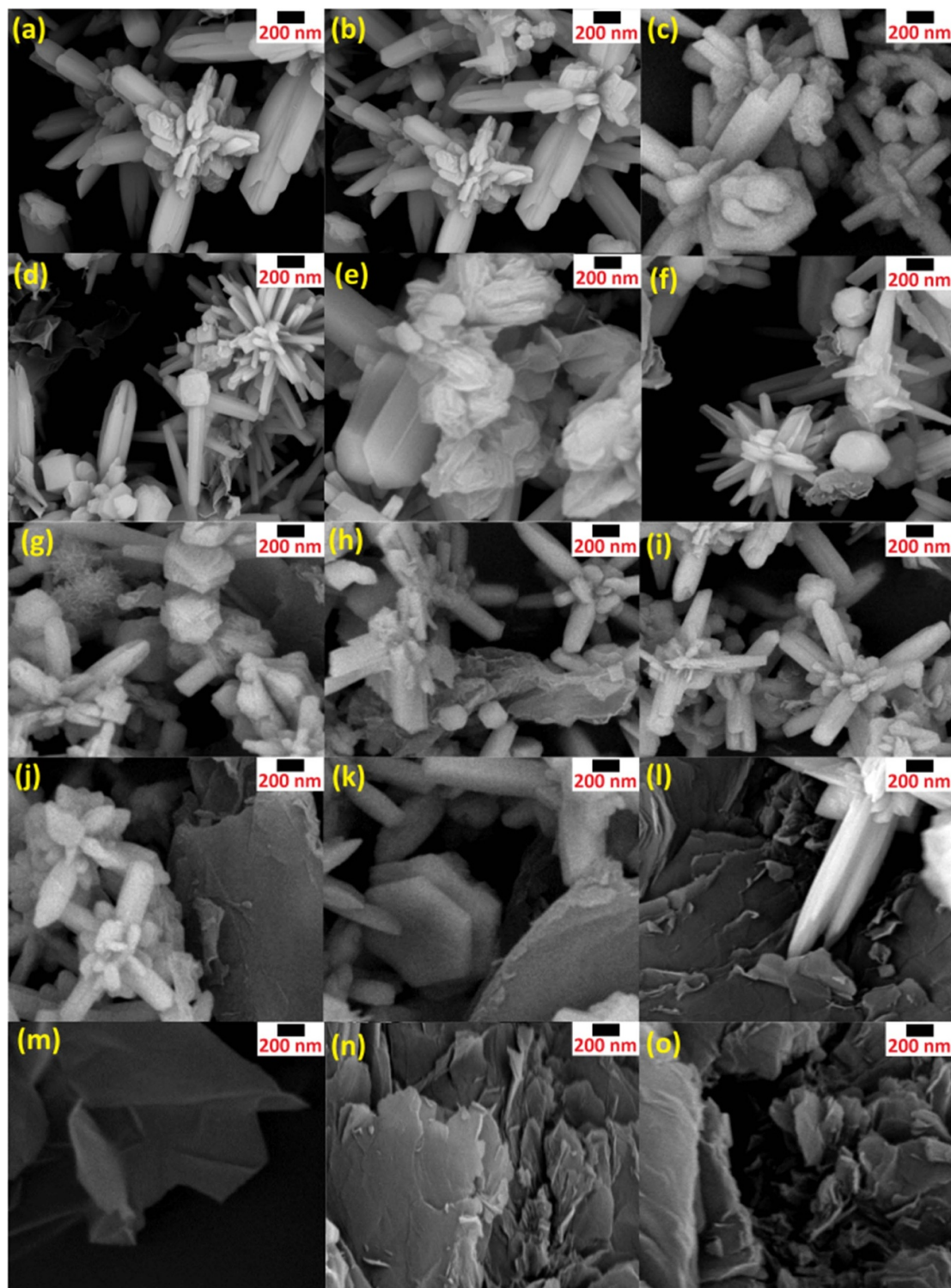


**Figure 2.** SEM images of NN (S1) (a)–(c), NNR (S2) (d)–(f), NNR (S3) (g)–(i), NNR (S4) (j)–(l), and rGO (m)–(o).

positive effect on the electrochemical process. The CV analysis of the NN catalyst shows a redox peak that is due to the conversion of  $\text{Ni}^{+3} \leftrightarrow \text{Ni}^{+2}$  [35]. We can see that adding rGO to the catalyst increases the peak intensity in the CV curve and improves the pseudocapacitive behavior of the catalyst in alkaline media.

The electrochemical properties of the catalysts were also investigated through electrochemical impedance spectroscopy (EIS) analysis. Measurements were made in the frequency range from 0.01 Hz to 100 kHz. Figure 5(b) compares the EIS spectra for NNR and NN. As can be seen, all the Nyquist plots of the EIS spectra consist of a rough semicircle in the high-frequency region followed by a linear component in the

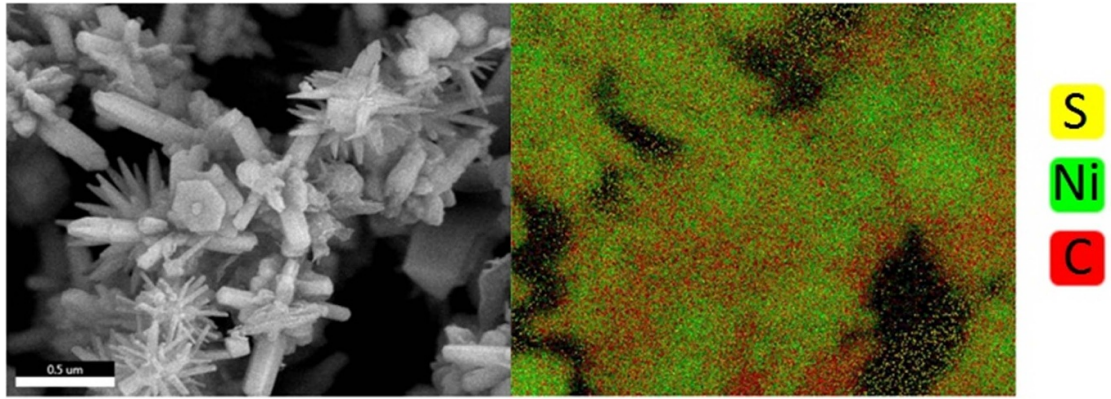


**Figure 3.** EDS mapping analysis of NNR (adapted from [34], copyright (2021), with permission from Elsevier). Reprinted from [34]. © 2021 Published by Elsevier Ltd.

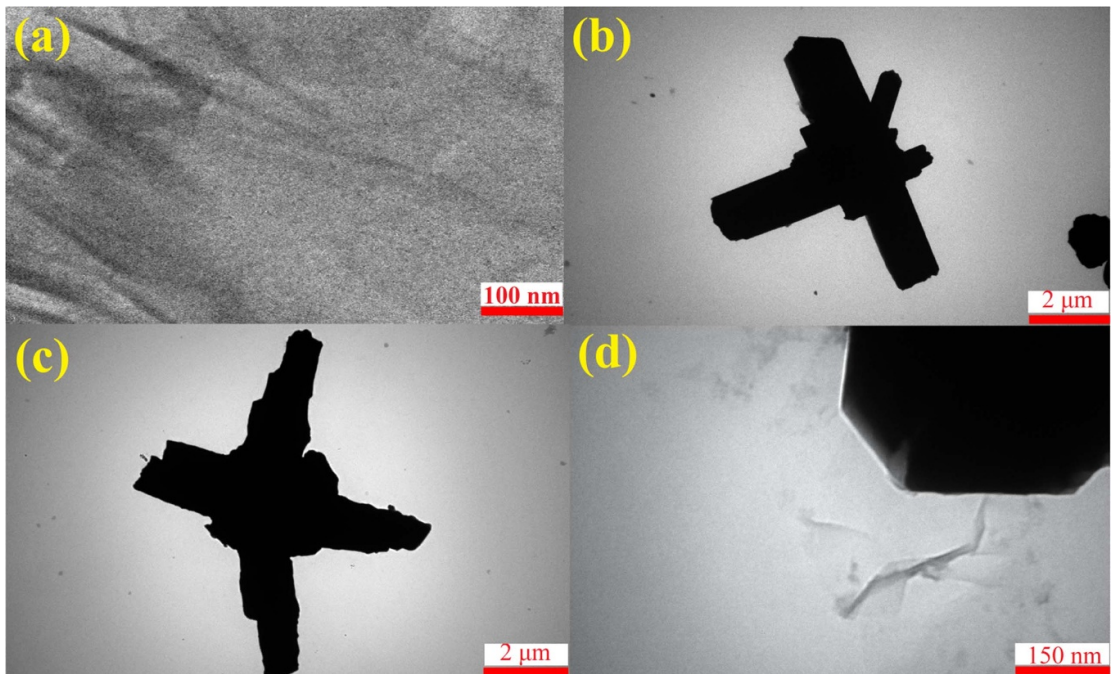


**Figure 4.** TEM images of rGO (a), NN (b), (c), and NNR (d) .

low-frequency region. The diameter of the semicircle indicates the surface charge transfer resistance ( $R_{ct}$ ) caused by Faraday reactions, which is lower in NNR than NN, at 12 and 16 ohms, respectively. According to the slope of the Warburg line, it can be concluded that the ion diffusion rate in NNR is higher than in NN, indicating higher electrochemically active sites in the catalyst.

According to figures 5(a) and (b), we can conclude that the NNR catalyst, having lower  $R_{ct}$  and higher current density, is a better performing catalyst than NN. However, the potential of both catalysts in the oxidation process of methanol and ethanol alcohols was evaluated.

To investigate the behavior of NN and NNR catalysts in the methanol oxidation process, a solution containing 1 M KOH and 0.1 M methanol was prepared. According to figure 6, both NN and NNR catalysts have relatively good potential in the MOR process. The behavioral comparison of these two catalysts indicates the apparent superiority of NNR in the MOR process. This advantage can be inferred from comparing the overvoltage and the maximum current density oxidation peak of the two catalysts. The maximum current density for NN is 8 and for NNR it is 15 mA cm<sup>-2</sup>, and the overvoltage for these catalysts is 400 and 420 mV, respectively. In the following, we intend to obtain the optimal concentration of methanol

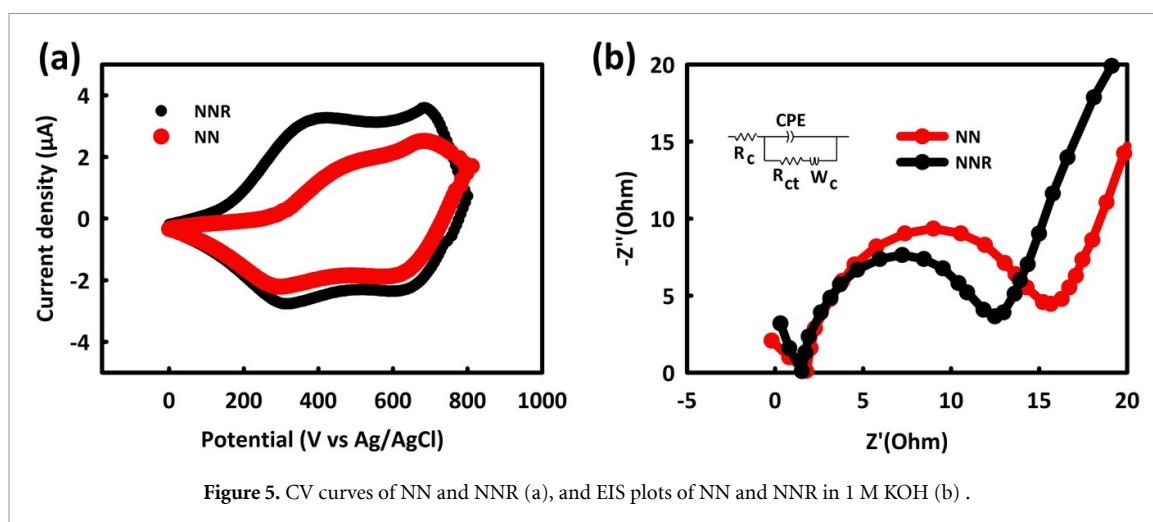


Figure 5. CV curves of NN and NNR (a), and EIS plots of NN and NNR in 1 M KOH (b).

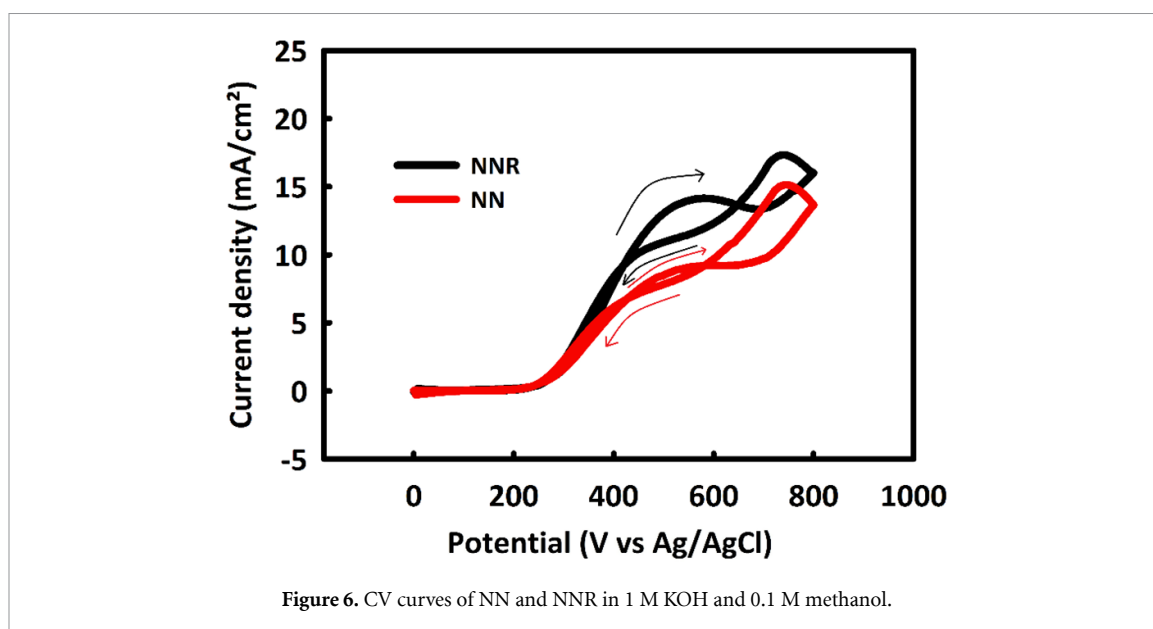


Figure 6. CV curves of NN and NNR in 1 M KOH and 0.1 M methanol.

and the optimal scan rate in the MOR process for the two catalysts. However, a solution containing 1 M KOH and different concentrations of methanol (0.1, 0.3, 0.5, 0.7, 0.9, and 1 molar of methanol) was prepared.

Figures 7(a) and (b) show the behavior of these two catalysts at different concentrations of methanol at a scan rate of  $10 \text{ mV s}^{-1}$ . In the MOR process with NN, the current density of methanol oxidation increases in the concentration of 0.5 M methanol, and from this concentration onwards, the current density decreases. Also, the current density variation trend for NNR increases up to a concentration of 0.7 M, and from this concentration onwards it decreases. This behavior is probably due to blocking the penetration of methanol into the catalyst core and preventing the MOR process by-products [36]. It can be concluded that rGO increases the active surface area of NNR and simultaneously causes delays in the saturation of the NNR surface by methanol oxidation by-products.

To obtain the optimal scan rate, the CV analysis of NN and NNR catalysts was performed at different scan rates and given concentrations. According to figure 7(c), by increasing the scan rate from  $10$  to  $60 \text{ mV s}^{-1}$ , the current density in the MOR process increases, but from  $60 \text{ mV s}^{-1}$  onwards, we see a decreasing trend in the current density. For NNR (figure 7(d)), we see an increase in the oxidation peak current density up to  $80 \text{ mV s}^{-1}$ , followed by a decrease in the  $100$  and  $120 \text{ mV s}^{-1}$  range. It seems that at higher scan rates than the optimal scan rate, the electrolyte and methanol do not have sufficient contact with the catalyst and do not penetrate deep into the catalyst core. The optimal scan rate in the methanol oxidation process for NNR is  $80 \text{ mV/s}$ , which is higher than NN ( $60 \text{ mV/s}$ ). rGO provides a more active surface area in the face of the electrolyte and methanol by enhancing more active electrochemical sites in the catalyst.

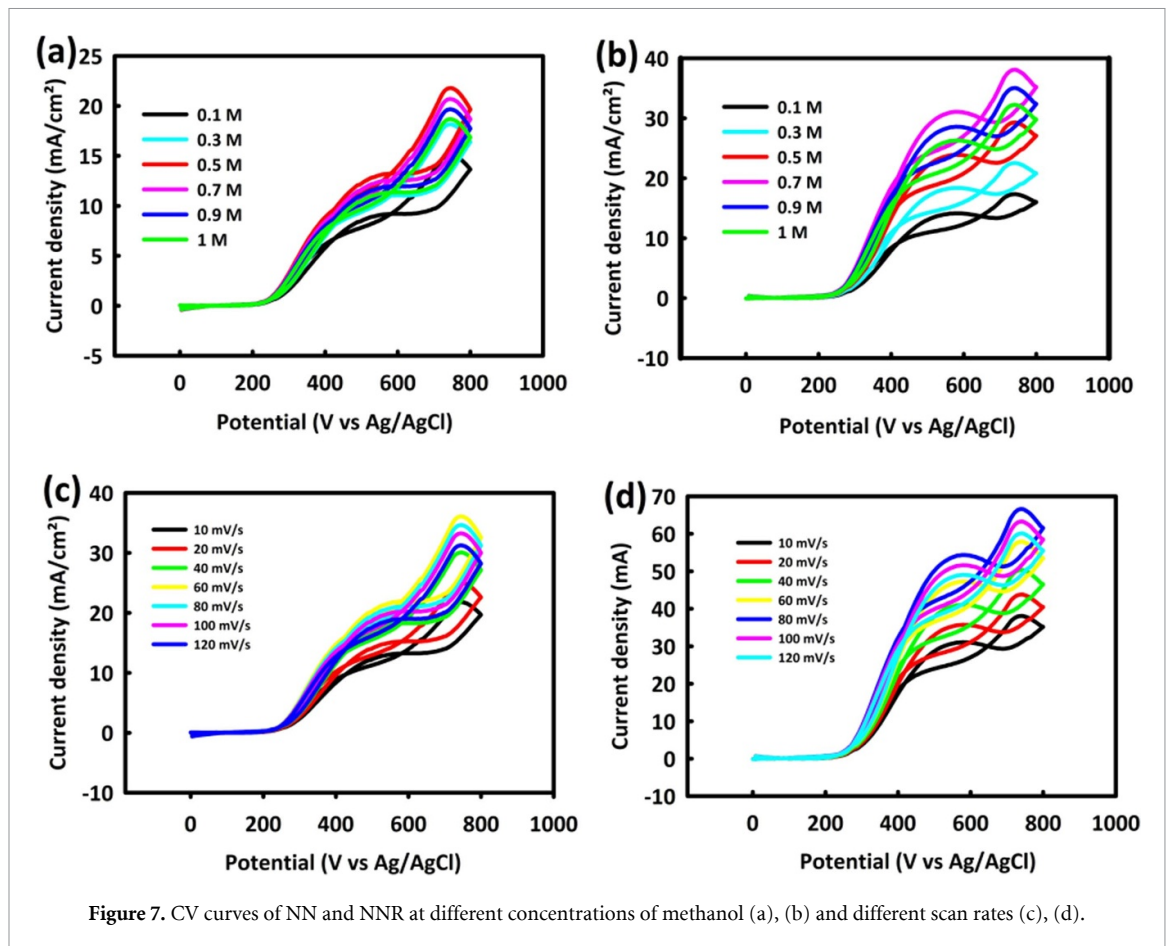
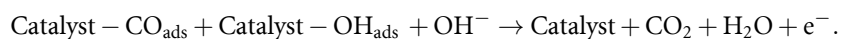
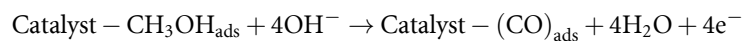
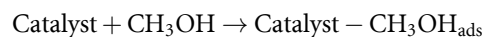


Figure 7. CV curves of NN and NNR at different concentrations of methanol (a), (b) and different scan rates (c), (d).

In many studies, the mechanism of methanol oxidation has been mentioned as a six-electron mechanism, and based on this, the MOR mechanism in the research is proposed as follows [37]:



To investigate the effect of temperature on the MOR process, CV analysis was performed at the optimal concentration and optimal scan rate at different temperatures (ambient temperature of 50 °C). As shown in figures 8(a) and (b), the oxidation peak for both catalysts increases with the increasing temperature. Methanol oxidation and the absorption of OH<sup>-</sup> seem to be facilitated by the increasing temperature.

The stability of the catalysts in the MOR process was evaluated by performing 1000 CV scans at the optimal concentration and optimal scan rate. As shown in figure 8(c), NN has a good cyclic stability of 92%, and this stability for NNR is 97% (figure 8(d)); both stability values are relatively acceptable. rGO increases the electrical conductivity and provides a high surface area for NNR, thus facilitating the MOR process at NNR in comparison with NN. In addition, in order to check the stability of the NNR catalyst in the methanol oxidation process, chronoamperometry analysis was performed at peak potential. As shown in the inset of figure 8(d), the catalyst maintains about 70% of the initial current density after 2000 s, which is a relatively acceptable amount.

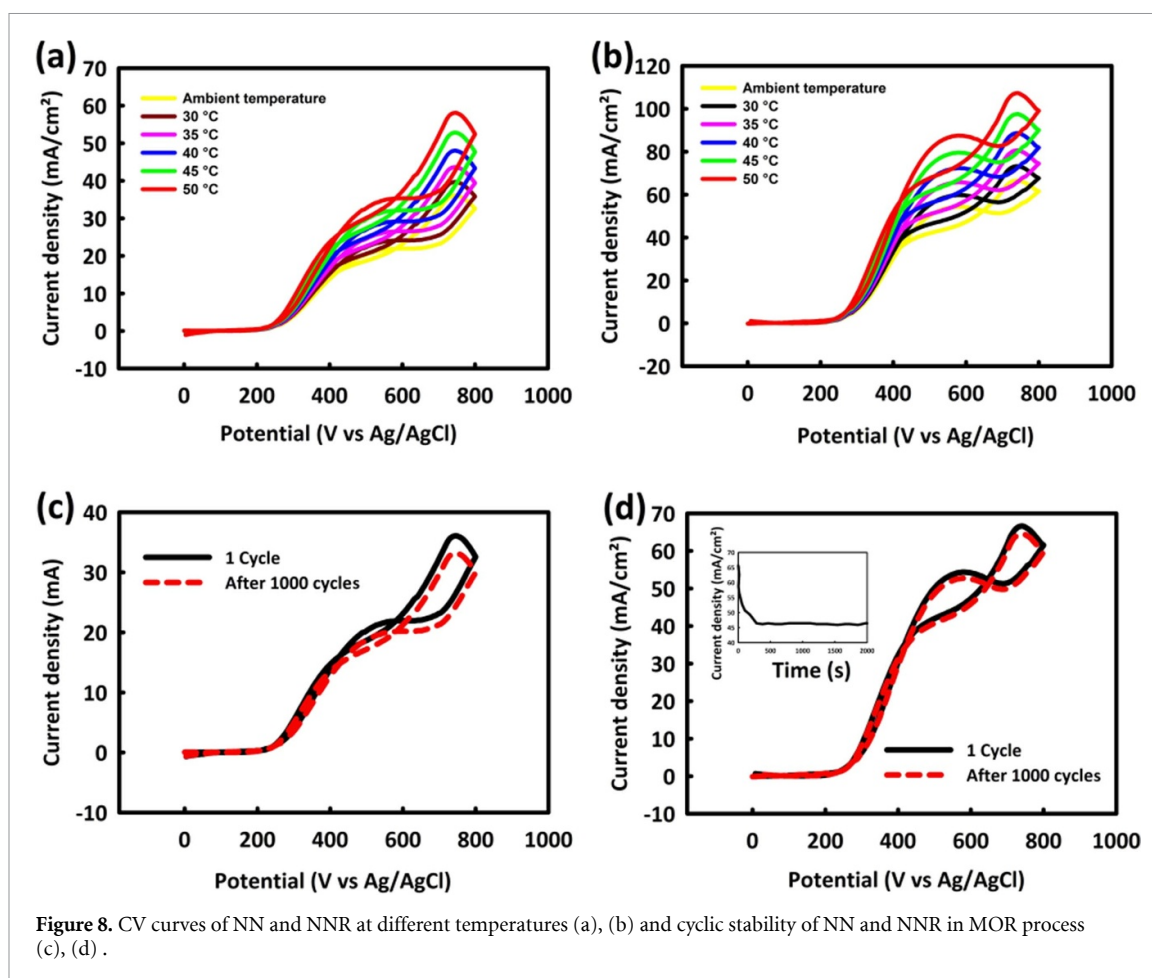


Figure 8. CV curves of NN and NNR at different temperatures (a), (b) and cyclic stability of NN and NNR in MOR process (c), (d).

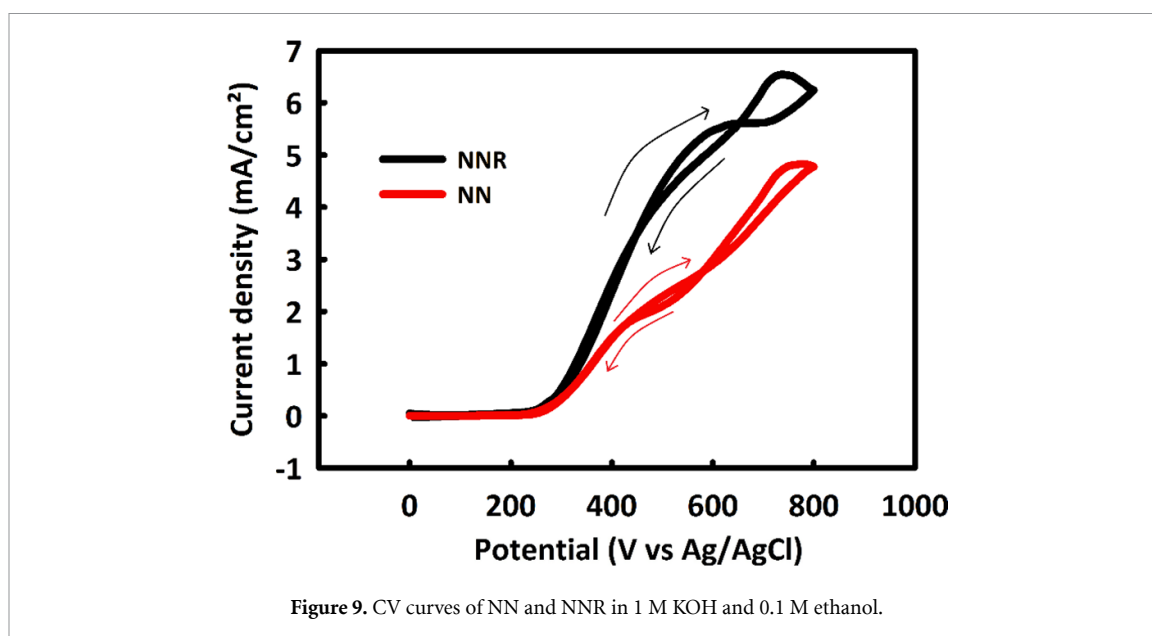


Figure 9. CV curves of NN and NNR in 1 M KOH and 0.1 M ethanol.

### 3.2. Electrochemical investigation of NN and NNR catalysts for the ethanol oxidation process

The ethanol oxidation capability of NN and NNR catalysts was evaluated by performing a CV test in an alkaline medium (figure 9). For this purpose, a solution consisting of 1 M KOH and 0.1 M ethanol was prepared. As shown in figure 8, the two catalysts are relatively capable of ethanol oxidation. Due to the stronger carbon bonds of ethanol than methanol, the oxidation of this alcohol by catalysts naturally occurs at higher overvoltages and lower current densities [38]. A comparison of NN and NNR behavior at different concentrations of ethanol was evaluated to obtain the optimal concentration by performing a CV test.

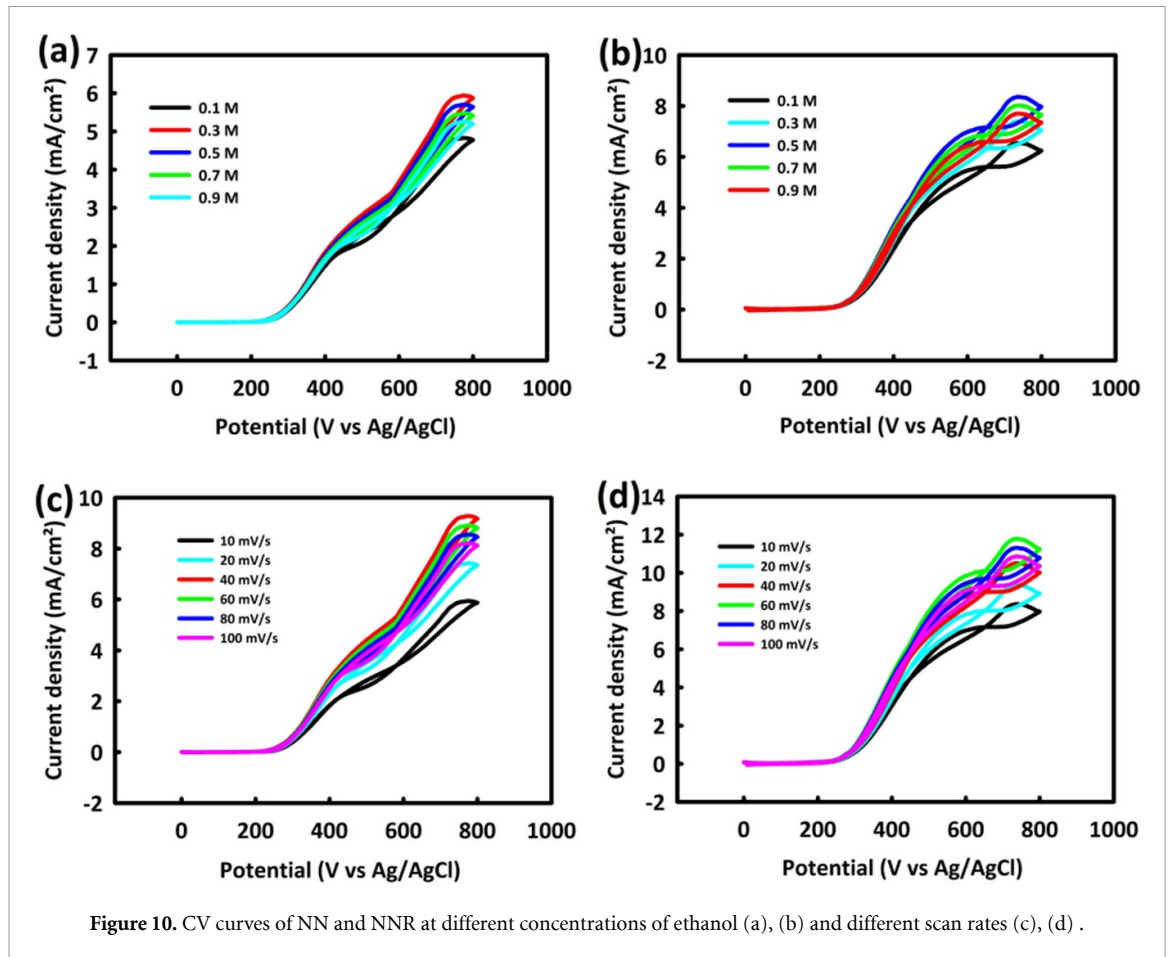


Figure 10. CV curves of NN and NNR at different concentrations of ethanol (a), (b) and different scan rates (c), (d) .

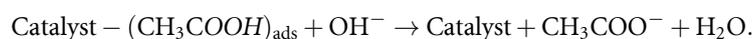
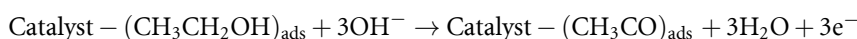
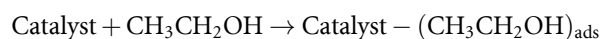
As shown in figures 10(a) and (b), the oxidation current density in NN and NNR catalysts increases to 0.3 and 0.5 methanol concentrations, respectively, and after these critical concentrations, we see a decrease in the peak current density with the saturation of the surface of the electrodes by the by-products of ethanol oxidation. In addition, the presence of rGO in the catalyst structure increases the surface area of the catalyst and delays the creation of contamination-affected by-products [39].

A CV test was performed using the optimal concentrations of ethanol at different scan rates, to obtain the optimal scan rate in the process of ethanol oxidation by two catalysts.

Figures 10(c) and (d) show that by changing the scan rate to 40 and 60 mV s<sup>-1</sup>, the peak oxidation current density has an upward trend, and from this scan rate onwards, it was decreased in NN and NNR, respectively.

In general, at scan rates higher than the optimal scan rate, the electrolyte and alcohol do not have enough opportunity to contact and penetrate deep into the catalyst, so the peak current density will be decreased.

The mechanism of the ethanol oxidation process by catalysts can be presented as follows [40]:



In the EOR process, we also see an increase in the current density with the increasing temperature. Figures 11(a) and (b) show that by increasing the temperature in the range of environments to 50 °C, the current density for both NN and NNR catalysts increases, and the ethanol oxidation process is facilitated by increasing the temperature.

The stability measurements of the two catalysts were also investigated by performing 1000 consecutive CV cycles at the optimal scan rate and concentration for NN and NNR in the EOR process.

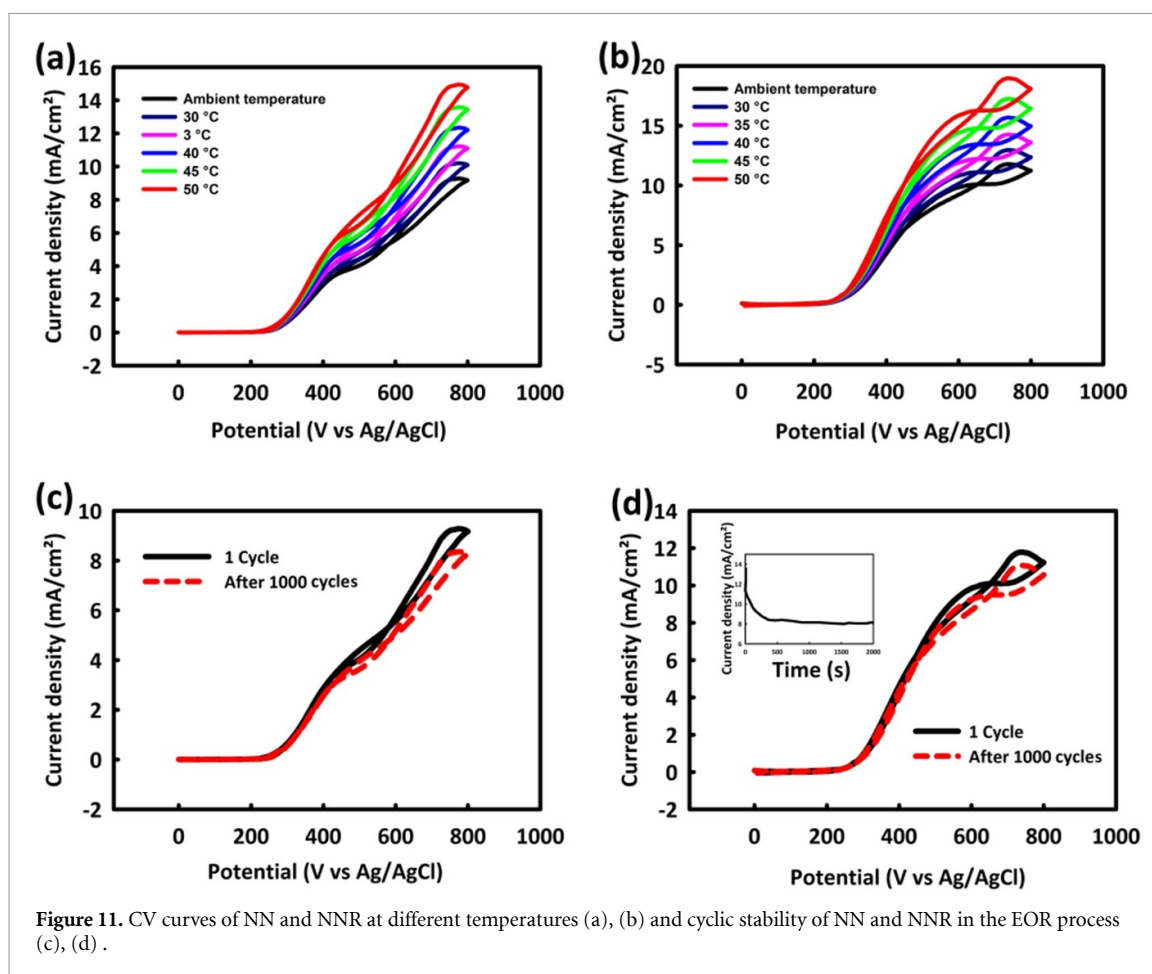


**Figure 11.** CV curves of NN and NNR at different temperatures (a), (b) and cyclic stability of NN and NNR in the EOR process (c), (d).

**Table 1.** Comparison of MOR and EOR performances for some reported electrocatalysts and the NNR in this work.

Electrocatalyst	Electrolyte composition	Peak potential (V)	Current density ( $\text{mA cm}^{-2}$ )	References
$\text{Ni}_3\text{S}_4$ -NiS-rGO	0.7 M MeOH/1 M KOH	0.54	55	This work
$\text{Ni}_3\text{S}_4$ -NiS-rGO	0.5 M EtOH/1 M KOH	0.59	11	This work
Ni-BTC/ $\text{NiS}_2$	1 M MeOH/0.1 M KOH	0.7	34.36	[41]
NiO/Ni-P	1 M MeOH/0.5 M KOH	0.5	28.56	[42]
$\text{NiMoO}_4$	2 M MeOH/1 M KOH	0.45	49	[43]
$\text{NiMoS}_2/\text{MXene}$	1 M MeOH/1 M KOH	0.75	7.7	[44]
$\text{NiCo}_2\text{O}_4$	0.5 M MeOH/1 M KOH	0.7	129	[45]
NF/ $\text{Co}_3\text{O}_4/\text{NiCo}_2\text{O}_4$	0.5 M MeOH/1 M KOH	0.6	140	[46]
$\text{MoS}_2/\text{Ni}_3\text{S}_2/\text{rGO}$	1 M MeOH/1 M KOH	0.4	80.04	[47]
$\text{Co}_3\text{O}_4$ - $\text{Ni}_3\text{S}_4$ -rGO	0.3 M MeOH/1 M KOH	0.4	52.9	[48]
Pd@Ni <sub>x</sub> B/ rGO	1 M EtOH/1 M KOH	-0.31	19.7	[49]
ZnO-MWCNT@ $\text{Fe}_3\text{O}_4$	0.5 M EtOH/1 M KOH	0.6	10	[50]
$\text{MnO}_2$ -NiO-MWCNTs	0.5 M EtOH/1 M KOH	0.55	$148 \mu\text{A cm}^{-2}$	[51]
$\text{Mn}_3\text{O}_4$ - $\text{CeO}_2$ -rGO	0.8 M MeOH/1 M KOH	0.51	17.7	[52]

As figure 11(c) indicates, after this number of consecutive cycles, NN still has a relatively good stability of 90% and NNR shows a stability of 94% (figure 11(d)) due to the role of rGO in its structure as a superior component for the creation of higher electrical conductivity and active surface area than NN. The stability of the NNR catalyst in the EOR process was determined by chronoamperometry analysis at the oxidation peak potential. As shown in the inset of figure 11(d), the catalyst maintains about 65% of the initial current density after 2000 s.

Table 1 compares the performance of the NNR catalyst in the methanol and ethanol oxidation process with other research.

## 4. Conclusion

In this study, we succeeded in synthesizing NN and NNR on the surface of NF using a one-step hydrothermal method. The electrochemical application of these catalysts with star-shaped morphology was performed through the alcohol oxidation process. The results show the relatively good ability of these catalysts in the oxidation of methanol and ethanol alcohols. NNR was introduced as a better and more effective catalyst than NN in the oxidation process of alcohols due to its higher active surface area and higher electrical conductivity. The presence of rGO in the metallic structure affected the surface of the NNR catalyst and created better stability in the oxidation of alcohols. The stability of NNR in MOR and EOR was measured as 97% and 94% respectively after 1000 consecutive cycles. The degree of stability in MOR and EOR was also evaluated by chronoamperometry analysis for NNR after 2000 s and at the oxidation peak potential. The amount of stability in the current density and in the methanol and ethanol oxidation processes was obtained as 70% and 65%, respectively. Based on the recent studies by researchers aimed at introducing inexpensive and stable catalysts for use in alcoholic fuel cells, NN and NNR are very promising for use in this field of study.

## Conflict of interest

The authors declare that there is no conflict of interest.

## Data availability statement

The data that support the findings of this study are available upon reasonable request from the authors.

## ORCID iDs

Sadeqh Azizi  <https://orcid.org/0000-0002-9716-2836>

Antonio Di Bartolomeo  <https://orcid.org/0000-0002-3629-726X>

## References

- [1] Mensah I A, Sun M, Gao C, Omari-Sasu A Y, Zhu D, Ampimah B C and Quarcoo A 2019 Analysis on the nexus of economic growth, fossil fuel energy consumption, CO<sub>2</sub> emissions and oil price in Africa based on a PMG panel ARDL approach *J. Clean. Prod.* **228** 161–74
- [2] Razmjoo A, Kaigutha L G, Rad M V, Marzband M, Davarpanah A and Denai M 2021 A technical analysis investigating energy sustainability utilizing reliable renewable energy sources to reduce CO<sub>2</sub> emissions in a high potential area *Renew. Energy* **164** 46–57
- [3] Kaur R, Marwaha A, Chhabra V A, Kim K-H and Tripathi S 2020 Recent developments on functional nanomaterial-based electrodes for microbial fuel cells *Renew. Sust. Energ. Rev.* **119** 109551
- [4] Palanisamy G, Jung H-Y, Sadhasivam T, Kurkuri M D, Kim S C and Roh S-H 2019 A comprehensive review on microbial fuel cell technologies: processes, utilization, and advanced developments in electrodes and membranes *J. Clean. Prod.* **221** 598–621
- [5] Wei C, Sun S, Mandler D, Wang X, Qiao S Z and Xu Z J 2019 Approaches for measuring the surface areas of metal oxide electrocatalysts for determining their intrinsic electrocatalytic activity *Chem. Soc. Rev.* **48** 2518–34
- [6] Kumar R, da Silva E T, Singh R K, Savu R, Alaferdov A V, Fonseca L C, Carossi L C, Singh A, Khandka S and Kar K K 2018 Microwave-assisted synthesis of palladium nanoparticles intercalated nitrogen doped reduced graphene oxide and their electrocatalytic activity for direct-ethanol fuel cells *J. Colloid Interface Sci.* **515** 160–71
- [7] Tian H, Yu Y, Wang Q, Li J, Rao P, Li R, Du Y, Jia C, Luo J and Deng P 2021 Recent advances in two-dimensional Pt based electrocatalysts for methanol oxidation reaction *Int. J. Hydrog. Energy* **46** 31202–15
- [8] Zakaria Z, Kamarudin S K, Abd Wahid K A and Hassan S H A 2021 The progress of fuel cell for Malaysian residential consumption: energy status and prospects to introduction as a renewable power generation system *Renew. Sust. Energy Rev.* **144** 110984
- [9] Zhang K, Wang H, Qiu J, Wu J, Wang H, Shao J, Deng Y and Yan L 2021 Multi-dimensional Pt/Ni(OH)<sub>2</sub>/nitrogen-doped graphene nanocomposites with low platinum content for methanol oxidation reaction with highly catalytic performance *Chem. Eng. J.* **421** 127786
- [10] Zhang R L, Duan J J, Han Z, Feng J J, Huang H, Zhang Q L and Wang A J 2020 One-step aqueous synthesis of hierarchically multi-branched PdRuCu nanoassemblies with highly boosted catalytic activity for ethanol and ethylene glycol oxidation reactions *Appl. Surf. Sci.* **506** 144791
- [11] Askari M B, Rozati S M, Salarizadeh P, Saeidirozesh H and Di Bartolomeo A 2021 A remarkable three-component RuO<sub>2</sub>-MnCo<sub>2</sub>O<sub>4</sub>/rGO nanocatalyst towards methanol electrooxidation *Int. J. Hydrog. Energy* **46** 36792–800
- [12] Baruah B and Kumar A 2021 Platinum-Free Anode Electrocatalysts for Methanol Oxidation in Direct Methanol Fuel Cells *Ceramic and Specialty Electrolytes for Energy Storage Devices* First Edition II (Boca Raton, FL: CRC Press) pp 261–83
- [13] Wang Q, Liu S, An S, Song X, Liang X, Wang Z and Mu Y 2021 Platinum nanoparticles assembled on different carbon materials and flower-like CeO<sub>2</sub> for methanol electro-oxidation *J. Mater. Sci., Mater. Electron.* **32** 26425–38
- [14] Durai L, Gunasekaran S S and Badhulika S 2022 A non-noble, low cost, multicomponent electrocatalyst based on nickel oxide decorated AC nanosheets and PPy nanowires for the direct methanol oxidation reaction *Int. J. Hydrog. Energy* **47** 3099–107
- [15] Gopalakrishnan A and Badhulika S 2021 Three-dimensional CoSe<sub>2</sub> nanoparticles/PANI films composite via co-electrodeposition as a binder-free and a non-noble metal catalyst alternative for methanol oxidation application *Mater. Chem. Phys.* **273** 125118

- [16] Sreekanth T, Tamilselvan M, Yoo K and Kim J 2021 Microwave-assisted *in situ* growth of VO<sub>2</sub> nanoribbons on Ni foam as inexpensive bifunctional electrocatalysts for the methanol oxidation and oxygen evolution reactions *Appl. Surf. Sci.* **570** 151119
- [17] Askari M B, Beheshti-Marnani A, Seifi M, Rozati S M and Salarizadeh P 2019 Fe<sub>3</sub>O<sub>4</sub>@MoS<sub>2</sub>/RGO as an effective nano-electrocatalyst toward electrochemical hydrogen evolution reaction and methanol oxidation in two settings for fuel cell application *J. Colloid Interface Sci.* **537** 186–96
- [18] Zhao X, Liu Q, Li Q, Chen L, Mao L, Wang H and Chen S 2020 Two-dimensional electrocatalysts for alcohol oxidation: a critical review *Chem. Eng. J.* **400** 125744
- [19] Askari M B, Salarizadeh P, Di Bartolomeo A, Beitollahi H and Tajik S 2021 Hierarchical nanostructures of MgCo<sub>2</sub>O<sub>4</sub> on reduced graphene oxide as a high-performance catalyst for methanol electro-oxidation *Ceram. Int.* **47** 16079–85
- [20] Zhang M, Song Z, Wang Z, Wang A, Zhu G and Shao S 2021 Platinum quantum dots enhance electrocatalytic activity of bamboo-like nitrogen doped carbon nanotubes embedding Co-MnO nanoparticles for methanol/ethanol oxidation *J. Colloid Interface Sci.* **590** 164–74
- [21] Yuan C Z, Sun Z T, Jiang Y F, Yang Z K, Jiang N, Zhao Z W, Qazi U Y, Zhang W H and Xu A W 2017 One-step *in situ* growth of iron–nickel sulfide nanosheets on FeNi alloy foils: high-performance and self-supported electrodes for water oxidation *Small* **13** 1604161
- [22] Wang P, Zhang X, Zhang J, Wan S, Guo S, Lu G, Yao J and Huang X 2017 Precise tuning in platinum-nickel/nickel sulfide interface nanowires for synergistic hydrogen evolution catalysis *Nat. Commun.* **8** 1–9
- [23] Lee M, Oh H S, Cho M K, Ahn J-P, Hwang Y J and Min B K 2018 Activation of a Ni electrocatalyst through spontaneous transformation of nickel sulfide to nickel hydroxide in an oxygen evolution reaction *Appl. Catal. B* **233** 130–5
- [24] Ouyang Y, Chen Y, Peng J, Yang J, Wu C, Chang B, Guo X, Chen G, Luo Z and Wang X 2021 Nickel sulfide/activated carbon nanotubes nanocomposites as advanced electrode of high-performance aqueous asymmetric supercapacitors *J. Alloys Compd.* **885** 160979
- [25] Shang X, Yan K L, Lu S S, Dong B, Gao W K, Chi J Q, Liu Z Z, Chai Y-M and Liu C G 2017 Controlling electrodeposited ultrathin amorphous Fe hydroxides film on V-doped nickel sulfide nanowires as efficient electrocatalyst for water oxidation *J. Power Sources* **363** 44–53
- [26] Arivazhagan M, Shankar A and Maduraiveeran G 2020 Hollow sphere nickel sulfide nanostructures–based enzyme mimic electrochemical sensor platform for lactic acid in human urine *Microchim. Acta* **187** 1–9
- [27] Li Q, Li L, Wu P, Xu N, Wang L, Li M, Dai A, Amine K, Mai L and Lu J 2019 Silica restricting the sulfur volatilization of nickel sulfide for high-performance lithium-ion batteries *Adv. Energy Mater.* **9** 1901153
- [28] Li S, He W, Liu B, Cui J, Wang X, Peng D L, Liu B and Qu B 2020 One-step construction of three-dimensional nickel sulfide-embedded carbon matrix for sodium-ion batteries and hybrid capacitors *Energy Storage Mater.* **25** 636–43
- [29] Ye C, Zhang L, Guo C, Li D, Vasileff A, Wang H and Qiao S Z 2017 A 3D hybrid of chemically coupled nickel sulfide and hollow carbon spheres for high performance lithium–sulfur batteries *Adv. Funct. Mater.* **27** 1702524
- [30] Hui L, Zhang X, Xue Y, Chen X, Fang Y, Xing C, Liu Y, Zheng X, Du Y and Zhang C 2022 Highly dispersed platinum chlorine atoms anchored on gold quantum dots for a highly efficient electrocatalyst *J. Am. Chem. Soc.* **144** 1921–8
- [31] He F and Li Y 2023 Advances on theory and experiments of the energy applications in graphdiyne *CCS Chem.* **5** 72–94
- [32] Zheng X, Li Y, Zhang L, Shen L, Xiao Y, Zhang Y, Au C and Jiang L 2019 Insight into the effect of morphology on catalytic performance of porous CeO<sub>2</sub> nanocrystals for H<sub>2</sub>S selective oxidation *Appl. Catal. B* **252** 98–110
- [33] Kumar R, Sahoo S, Joanni E, Singh R K, Tan W K, Kar K K and Matsuda A 2019 Recent progress in the synthesis of graphene and derived materials for next generation electrodes of high performance lithium ion batteries *Prog. Energy Combust. Sci.* **75** 100786
- [34] Darsara S A, Seifi M, Askari M B and Osquian M 2021 Hierarchical 3D starfish-like Ni<sub>3</sub>S<sub>4</sub>–NiS on reduced graphene oxide for high-performance supercapacitors *Ceram. Int.* **47** 20992–8
- [35] Tian D, Chen S, Zhu W, Wang C and Lu X 2019 Metal–organic framework derived hierarchical Ni/Ni<sub>3</sub>S<sub>2</sub> decorated carbon nanofibers for high-performance supercapacitors *Mater. Chem. Front.* **3** 1653–60
- [36] Tomboc G M, Abebe M W, Baye A F and Kim H 2019 Utilization of the superior properties of highly mesoporous PVP modified NiCo<sub>2</sub>O<sub>4</sub> with accessible 3D nanostructure and flower-like morphology towards electrochemical methanol oxidation reaction *J. Energy Chem.* **29** 136–46
- [37] Askari M B, Salarizadeh P, Seifi M and Rozati S M 2019 Electrocatalytic properties of CoS<sub>2</sub>/MoS<sub>2</sub>/rGO as a non-noble dual metal electrocatalyst: the investigation of hydrogen evolution and methanol oxidation *J. Phys. Chem. Solids* **135** 109103
- [38] Ruiz-Camacho B, Medina-Ramirez A, Aguilera M V and Minchaca-Mojica J 2019 Pt supported on mesoporous material for methanol and ethanol oxidation in alkaline medium *Int. J. Hydrog. Energy* **44** 12365–73
- [39] Noor T, Zaman N, Nasir H, Iqbal N and Hussain Z 2019 Electro catalytic study of NiO-MOF/rGO composites for methanol oxidation reaction *Electrochim. Acta* **307** 1–12
- [40] Askari M B, Salarizadeh P, Beheshti-Marnani A and Di Bartolomeo A 2021 NiO-Co<sub>3</sub>O<sub>4</sub>-rGO as an efficient electrode material for supercapacitors and direct alcoholic fuel cells *Adv. Mater. Interfaces* **8** 2100149
- [41] Luo J Y, Hu F C, Xi B J, Han Q W, Wu X Q, Wu Y P, Zhang Q, Chi R and Li D-S 2022 Fabricating of Ni-BTC/NiS<sub>2</sub> heterostructure via self-assembly strategy for electrocatalytic methanol oxidation *Inorg. Chem. Commun.* **143** 109777
- [42] Tong Y, Gu C, Zhang J, Tang H, Wang X and Tu J 2016 Thermal growth of NiO on interconnected Ni–P tube network for electrochemical oxidation of methanol in alkaline medium *Int. J. Hydrog. Energy* **41** 6342–52
- [43] Jothi P R, Kannan S and Velayutham G 2015 Enhanced methanol electro-oxidation over *in-situ* carbon and graphene supported one dimensional NiMoO<sub>4</sub> nanorods *J. Power Sources* **277** 350–9
- [44] Chandran M, Raveendran A, Vinoba M, Vijayan B K and Bhagiyalakshmi M 2021 Nickel-decorated MoS<sub>2</sub>/MXene nanosheets composites for electrocatalytic oxidation of methanol *Ceram. Int.* **47** 26847–55
- [45] Das A K, Jena S, Sahoo S, Kuchi R, Kim D, Aljohani T A, Nayak G C and Jeong J-R 2020 Facile synthesis of NiCo<sub>2</sub>O<sub>4</sub> nanorods for electrocatalytic oxidation of methanol *J. Saudi Chem. Soc.* **24** 434–44
- [46] Qian L, Luo S, Wu L, Hu X, Chen W and Wang X 2020 *In situ* growth of metal organic frameworks derived hierarchical hollow porous Co<sub>3</sub>O<sub>4</sub>/NiCo<sub>2</sub>O<sub>4</sub> nanocomposites on nickel foam as self-supported flexible electrode for methanol electrocatalytic oxidation *Appl. Surf. Sci.* **503** 144306
- [47] Salarizadeh P, Askari M B and Di Bartolomeo A 2022 MoS<sub>2</sub>/Ni<sub>3</sub>S<sub>2</sub>/Reduced graphene oxide nanostructure as an electrocatalyst for alcohol fuel cells *ACS Appl. Nano Mater.* **5** 3361–73
- [48] Askari M B and Rozati S M 2022 Construction of Co<sub>3</sub>O<sub>4</sub>-Ni<sub>3</sub>S<sub>4</sub>-rGO ternary hybrid as an efficient nanoelectrocatalyst for methanol and ethanol oxidation in alkaline media *J. Alloys Compd.* **900** 163408

- [49] Krishna R, Fernandes D M, Ventura J, Freire C and Titus E 2016 Facile synthesis of reduced graphene oxide supported Pd@Ni<sub>3</sub>B/RGO nanocomposite: novel electrocatalyst for ethanol oxidation in alkaline media *Int. J. Hydrog. Energy* **41** 11811–22
- [50] Moghadam M T T, Seifi M, Askari M B and Azizi S 2022 ZnO-MWCNT@ Fe<sub>3</sub>O<sub>4</sub> as a novel catalyst for methanol and ethanol oxidation *J. Phys. Chem. Solids* **165** 110688
- [51] Shojaeifar M, Askari M B, Hashemi S R S and Di Bartolomeo A 2022 MnO<sub>2</sub>-NiO-MWCNTs nanocomposite as a catalyst for methanol and ethanol electrooxidation *J. Appl. Phys.* **55** 355502
- [52] Askari M B, Rozati S M and Di Bartolomeo A 2022 Fabrication of Mn<sub>3</sub>O<sub>4</sub>-CeO<sub>2</sub>-rGO as nanocatalyst for electro-oxidation of methanol *Nanomaterials* **12** 1187